Microdroplet PhotoFuel Cells to Harvest High Density Energy and Dye Degradation

Siddharth Thakur,[a] Nayan Mani Das,[b] Sunny Kumar,[a] Ashok Kumar Dasmahapatra†[ab] and Dipankar Bandyopadhyay†[ab]

[a]Department of Chemical Engineering, Indian Institute of Technology Guwahati, India
[b]Centre for Nanotechnology, Indian Institute of Technology Guwahati, India.

Keywords: Microdroplet; Fuel cell; Dye degradation; Plasmons; Nanoparticles

Corresponding Authors: dipban@iitg.ac.in, Tel - +91 361 258 2254, akdm@iitg.ac.in, Tel - +91 361 258 2254

I. FETEM and UV-Vis spectra of Au/CdS nanocomposites

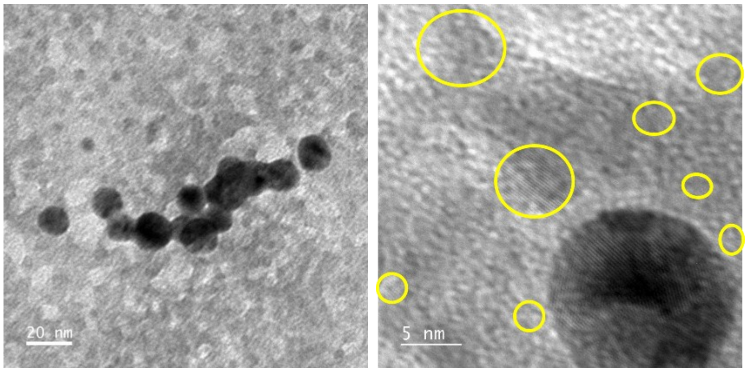

Figure S1: FETEM images of Au and CdS NPs. Image (a) shows the average size of AuNPs to be ~15 nm to 20 nm. Image (b) shows the HRTEM image of the Au (darker patch) and CdS NPs (encircled).

The FETEM images of the Au and CdS NPs have been shown in the **Figure S1**. The smaller CdS NPs (lighter gray shade) compose the base surface on which the islands of the Au NPs (darker gray shade) form a composite arrangement. The UV-Visible spectroscopy was used to characterize the stability of the Au-CdS nanocomposite after peroxide treatment.

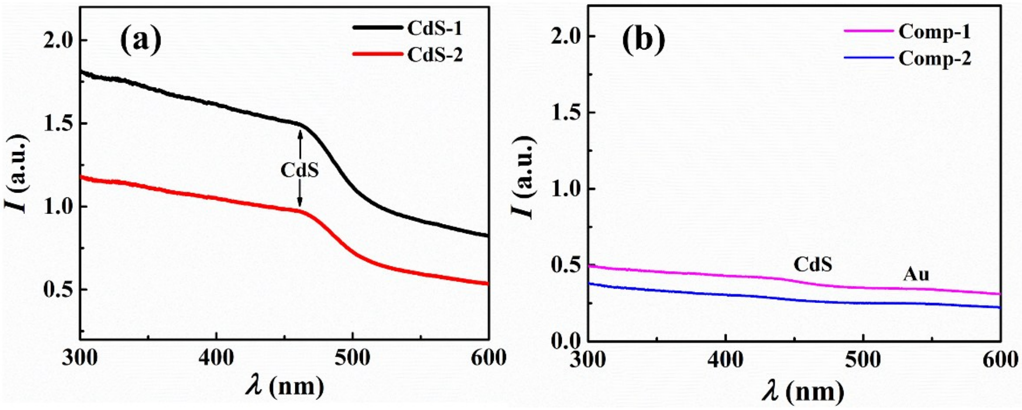

Figure S2: The UV-Visible spectroscopy of bare CdS NPs and Au/CdS NPs in the presence of H_2O_2. In image (a), CdS-1 and CdS-2 refers to UV-Visible spectra of CdS NP before and after treatment with H_2O_2. In the image (b) Au/CdS-1 and Au/CdS-2 refers to UV-Visible spectra of Au/CdS NPs before and after treatment with H_2O_2.

The plots (a) and (b) in the **Figure S2** show the characteristic peaks of Au (520 nm) and CdS (450 nm) before and after the treatment with peroxide fuel. The plot (a) shows that the CdS peak intensity (as depicted in the ordinate values of the plot) drastically decreased and there was a peak shift due to the oxidation of CdS to $CdSO_4$ during peroxide treatment. However, for the other case in the plot (b) we observe that there is a slight decrease in the peak intensity with a negligible shift in peak wavelength thereby verifying the stability of the Au-CdS nanocomposites against H_2O_2.

II. *P*-*ψ* for Native Setup and Effect of pH

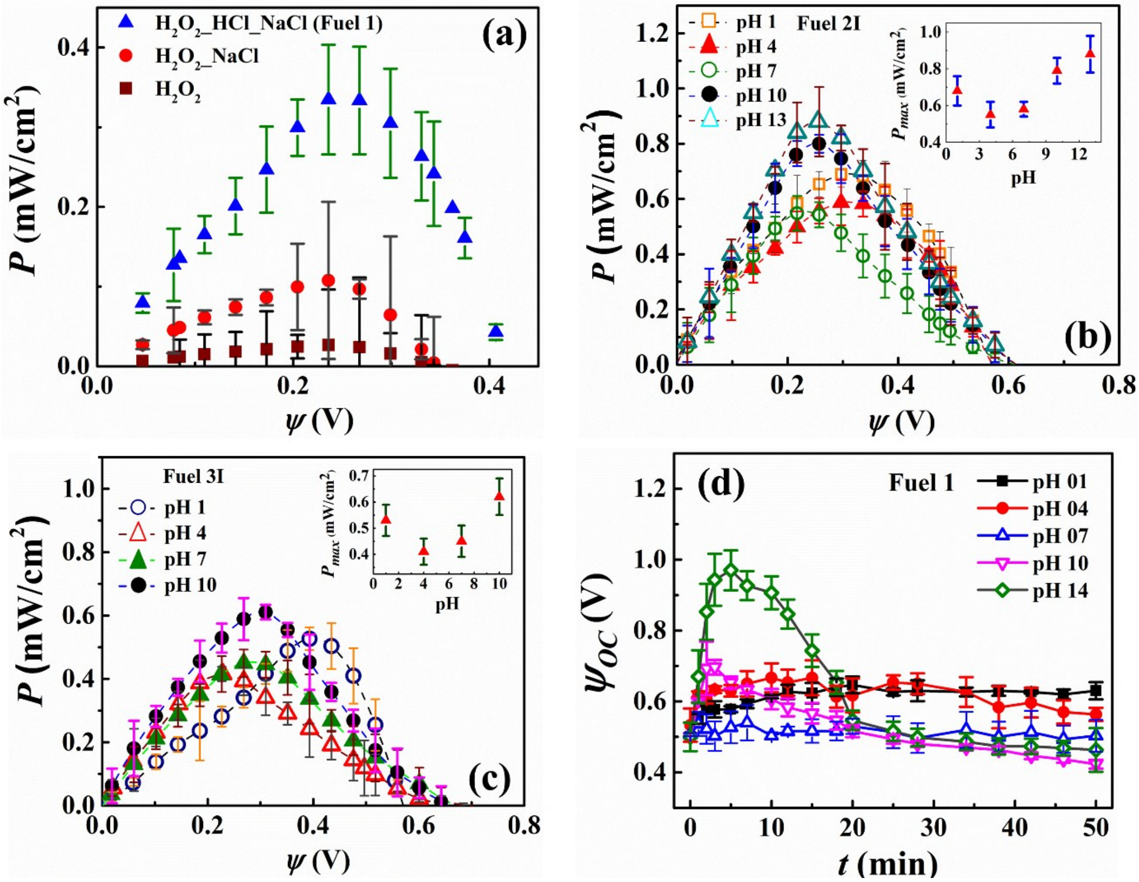

Figure S3: Image (a) shows the *P*-*ψ* characteristics of a few native μ-DropFC setups, which comprise of three different solutions, (i) 10 μL of 0.3M aqueous H_2O_2 and 10 μL of 0.1M HCl, (ii) a 20 μL droplet obtained by mixing 10 μL aqueous 0.3M H_2O_2 with 10 μL of aqueous 0.1M HCl, and (iii) 30 μL of fuel 1 – mixing 10 μL aqueous H_2O_2 (0.3 M) with 10 μL aqueous HCl (0.1 M) and 10 μL aqueous NaCl (1M). Images (b) and (c) show the effect of pH on the *P*-*ψ* plots of the 10 μL droplet of Fuels 2I and 3I. Image (d) shows the variation of ψ_{oc} of Fuel 1 at different pH.

A few major parameters associated with the μ-DropFC setups were the pH of the droplet, electrical conductivity of the droplet, maximum power generated (P_{max}) and open circuit voltage (ψ_{oc}). **Figure S3** shows the results obtained during the tuning of all these parameters to extract an optimal performance from the native μ-DropFC, before the addition of the nanoparticles. It may be noted here that all these experiments were carried out under illuminated conditions. The plot (a) shows the *P*-*ψ* characteristics of three different solutions, (i) 10 μL of 0.3M aqueous H_2O_2, (ii) a 20 μL droplet obtained by mixing 10 μL aqueous 0.3M H_2O_2 with 10 μL of aqueous 0.1M HCl, and (iii) 30 μL of Fuel 1 – mixing 10 μL aqueous H_2O_2 (0.3 M) with 10 μL aqueous HCl (0.1 M) and 10 μL aqueous NaCl (1M). All the P-ψ plots in the images (a) – (c) show a progressive increase in P with ψ until they reach a maximum value of P_{max} before they progressively decreased with the increase in ψ to arrive at ψ_{oc}.

The plots suggest that since the pristine 0.3M aqueous H_2O_2 was itself a highly reactive medium, it decomposed rapidly due to the interaction with the electrode materials and photonic excitations. However, as suggested by the blue P-ψ plot in the plot (a), this system was unable to generate significant power. It may be noted here that the H_2O_2 procured always contained some amount of HCl during its supply to maintain its stability during transport under dark condition. Importantly, when we increased the stability of the H_2O_2 procured by mixing the same with 0.1M aqueous HCl solution, the presence of the H^+ ions in the solution negatively catalyzed the system to provide further stability. In such a scenario, the μ-DropFC decomposed with a significant rate for a longer duration when integrated with the electrodes and exposed to light, which helped in improving P_{max} and ψ_{oc}, as shown in the plot (a). The cell characteristics could be improved further when the aqueous NaCl solution was added to the system. Subsequently, a 30 μL droplet of μ-DropFC at pH 1 and in presence NaCl produced a P_{max} ~ 0.35 mW/cm^2 and 0.38 V. This we have chosen as the native system for all other experiments and named as Fuel 1 in the main manuscript.

Importantly, the μ-DropFC performance varied significantly with the pH of the droplet. The plots (b) and (c) in the **Figure S3** depict the P-ψ measurements of Fuels 2I and 3I of the main manuscript, respectively, when pH was varied from 1 to 13. The inset in the plots show the variations in P_{max} with pH. It may be noted here that the alkalinity (acidity) of the solutions was varied by adding aqueous NaOH (HCl) solution before measuring the pH with pH meter. The plots show that P_{max} could be improved significantly with the increase in the alkalinity of the solutions for the Fuels 2 and 3. It is well known that the OH^- positively catalyzes peroxide decomposition, which could be further aided by Au and CdS NPs. The highly alkaline solutions not only degraded the fuel quickly but also neutralized the Au/CdS NP. However, the major issues associated with the alkaline system were smaller shelf-life and marginal ψ_{oc}, which has been summarized in the plot (d) of **Figure S3** for the Fuel 1. The reactive decomposition of H_2O_2 under alkaline condition can be shown in the following way:[1]

$$H_2O_2 + OH^- \rightarrow HO_2^- + H_2O\,, \tag{1}$$

$$HO_2^- + H_2O + 2e^- \rightarrow 3OH^-,$$ (2)

$$HO_2^- + OH^- \rightarrow O_2 + H_2O + 2e^-,$$ (3)

$$O_2 + 2H_2O + 4e^- \rightarrow 4OH^-.$$ (4)

The plot (d) shows that ψ_{oc} varied with time (t) considerably for solutions with different pH. At higher pH values, peroxide existed as hydroperoxyl ions in the solution, as shown below in Eq. (1). These ions then combined with water to give hydroxyl ions, as shown in Eq. (2). In these highly alkaline conditions, sudden increase in the ψ_{oc} was observed because the change in the concentration of OH^- ions facilitated faster breakdown of H_2O_2, as shown in the Eq. (3). Moreover, since oxygen was present, its reduction could also take place at such potential values following the Eq. (4). Thus, such alkaline conditions were found not so sustainable for long-term power generation because the rapid degradation of peroxide due to combination with the reactive oxygen species (ROS).

On the other hand, at low pH values, the hydrogen peroxide was more stable as the reactive species were generally kept under control, which led to a much more consistent ψ_{oc}. The decomposition of peroxide fuel in acidic media can be shown by the following equations:[1]

$$H_2O_2 + 2H^+ + 2e^- \rightarrow 2H_2O,$$ (5)

$$H_2O_2 \rightarrow O_2 + 2H^+ + 2e^-,$$ (6)

$$O_2 + 4H^+ + 4e^- \rightarrow 2H_2O.$$ (7)

Over longer periods of time, these conditions were found to be favorable for a controlled decomposition of peroxide fuel, which led to a higher ψ_{oc} value compared to the alkaline conditions, as shown by the black line in the plot (d) of **Figure S3**. This mechanisms for this phenomenon is also a well-established one in the existing literature.[2,3] Under such conditions, the H_2O_2 molecules reduced at the electrodes into water in the presence of charges, as shown in Eq. (5). Subsequently, at these potential values, H_2O_2 oxidation could also take place at the anode, as shown in the Eq. (6). Since, oxygen was also present in the system, it also reduced at the electrodes, as shown in Eq. (7), which was the main cause of the increased overpotential and decrease in the overall ψ_{oc} values. Concisely, the plots (a) – (d) in the **Figure S3** suggests that pH 1 was the optimal for significant power generation at an adequate open circuit voltage for the proposed μ-DropFC, which justified the usage of Fuel 1 as the native system for all the experiments performed in the main manuscript. Subsequently, all the other Fuels 2 – 6 were synthesized by mixing Au or CdS NPs or dyes with the Fuel 1, as summarized in the Table 1 of the main manuscript.

III. Electrode Characterization

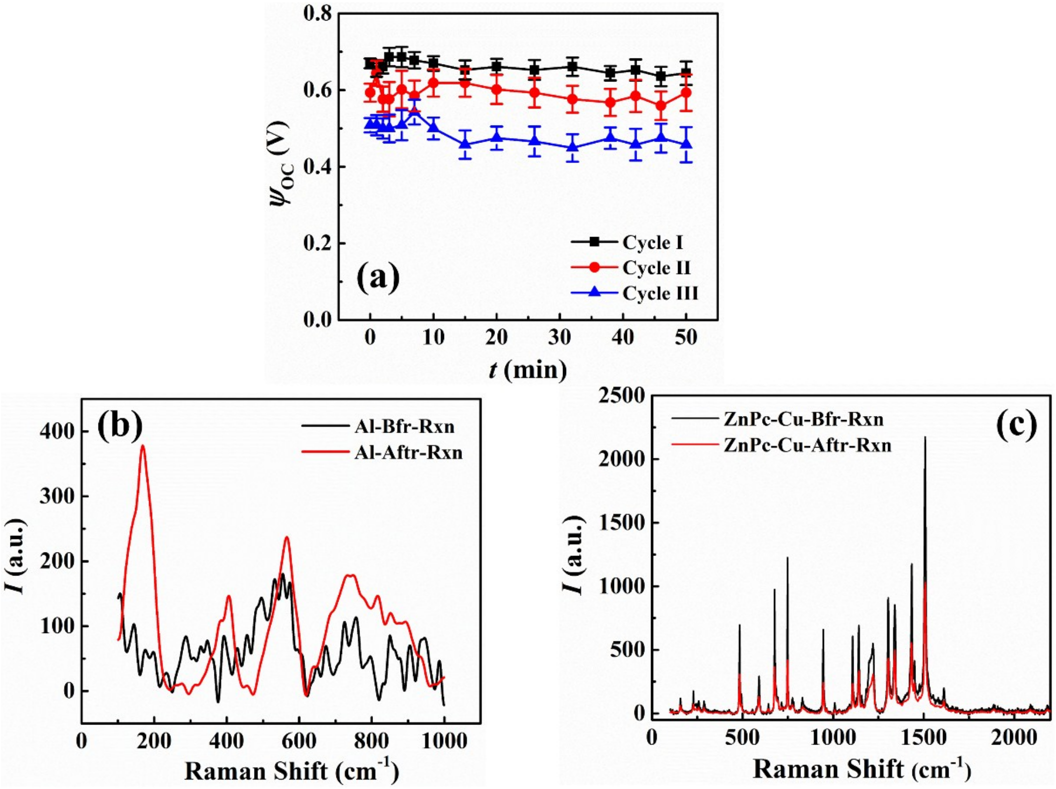

Figure S4: Image (a) shows variation of ψ_{oc} with t of the Fuel 2I when the electrodes were utilized for three times. Image (b) shows the Raman spectra of the Al anode before (Al-Bfr-Rxn) and after the reaction (Al-Aftr-Rxn). Image (c) shows the same for ZnPC-Cu cathode before (ZnPC-Cu-Bfr-Rxn) and after (ZnPC-Cu-Aftr-Rxn) reaction.

The electrode degradation was characterized by Raman spectra, as summarized in the **Figure S4**. The plot (a) shows the variation of ψ_{oc} with t of the Fuel 2I when integrated with the same set of electrodes for 3 cycles each spanning 50 min. The plot suggests that after each cycle the degradation was not that significant and even after 150 min of operation, the change in the ψ_{oc} was not that significant. In these experiments, as soon as peroxide touched the Al surface, the peroxide decomposition led to the etching of Al surface to form $Al(OH)_3$. This anodic oxidation was one of the major reasons behind the reduction of ψ_{oc} in each cycle, which prevented charge transfer to some extent. The plot (b) show the Raman spectra of the anode before and after the reaction. After a reaction time of 50 min, new peaks were observed on the Al surface owing to the formation of the hydroxide layer.[4] The plot also shows that the variation in the spectra was not that significant and the electrode could be used further for performing experiments. Importantly, the cathode surface did not change much due to the chemical stability of the ZnPC on Cu, as shown in the plot (c).

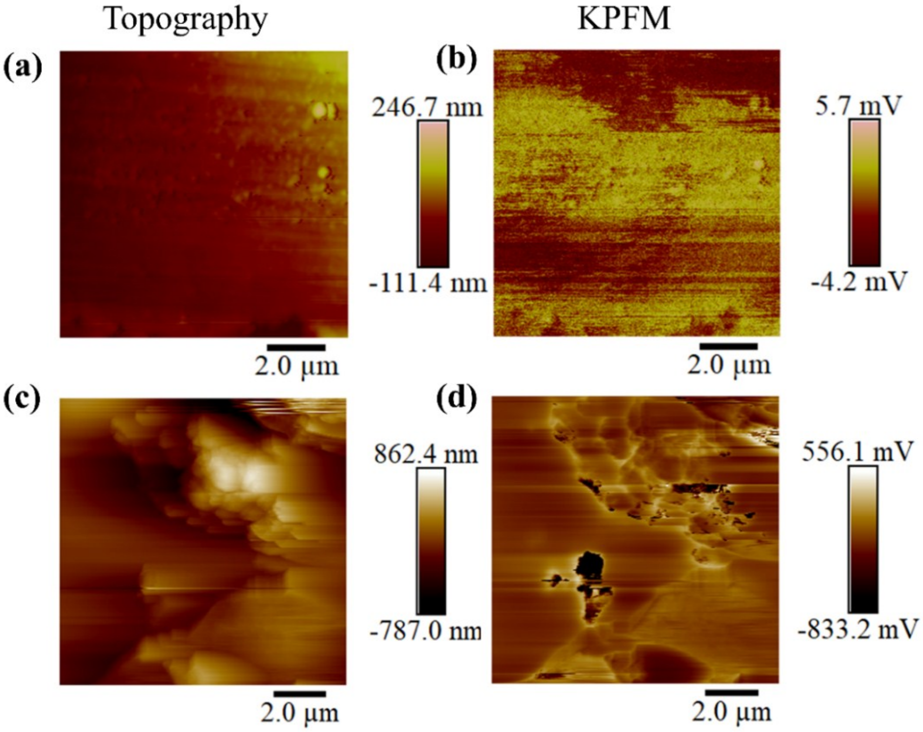

Figure S5: Image (a) shows the topographic profile of the unused Al foil electrode. Image (b) shows the corresponding surface potential plot of the Al foil electrode. Image (c) shows the surface profile of the Al foil electrode after exposure to peroxide solution in the presence of an anodic bias. Image (d) shows the corresponding surface potential profile of the reacted Al foil electrode.

We also determined the change in surface potential using the Kelvin Probe Force Microscopy (KPFM) of the electrodes before and after the exposure of H_2O_2. In the topography AFM image, plot (a) of **Figure S5,** a clear surface belonging to the unused Al foil electrode could be observed along with its respective surface potential, as shown in plot (b). However, after the exposure to peroxide solution in the presence of an anodic bias, the change in the topography as well as the surface potential could be visible in the images (c) and (d). The images suggest the surface topography and potential changed significantly due to the chemical reaction between peroxide and electrode. In order to further understand this observation, we have employed the KPFM model to investigate the change in work function of the electrodes in the presence of corrosive material. A modulation voltage of 0.5 V was maintained in between the cantilever and the sample surface to attain a resonance frequency of cantilever in order to map the surface potential over the Al foil electrode. A Pt/Ir coated Si tip whose work function had been optimized to be 4.58 eV by using the known work function of a HOPG surface had been used for the analysis. We could quantitatively measure the surface potential by applying the following equation:

$$CPD = \left(\phi_{tip} - \phi_{sample}\right) / e. \tag{8}$$

The KPFM aids in the determination of the contact potential difference (CPD) between the work function of the tip (ϕ_{tip}) and the work function of the material (ϕ_{sample}) when, *e*, is the elementary electronic charge. From the calculations using the software nanoscope analysis, the CPD of the unused Al foil electrode was calculated to be ~0.0033 eV, as represented by plot (b). Therefore, using the above equation, the work function of the electrode before applying the peroxide solution was found to be 4.577 eV. After the Al foil electrode was exposed to the peroxide solution in presence of an anodic bias, the CPD of the substrate changed by ~ 0.545 eV, as represented by plot (d). Thus, after applying the equation mentioned above, the work function of the electrode after the exposure of peroxide was found to be 5.125 eV.

IV. *P*-*ψ* for μ-DropFC with Rh6G

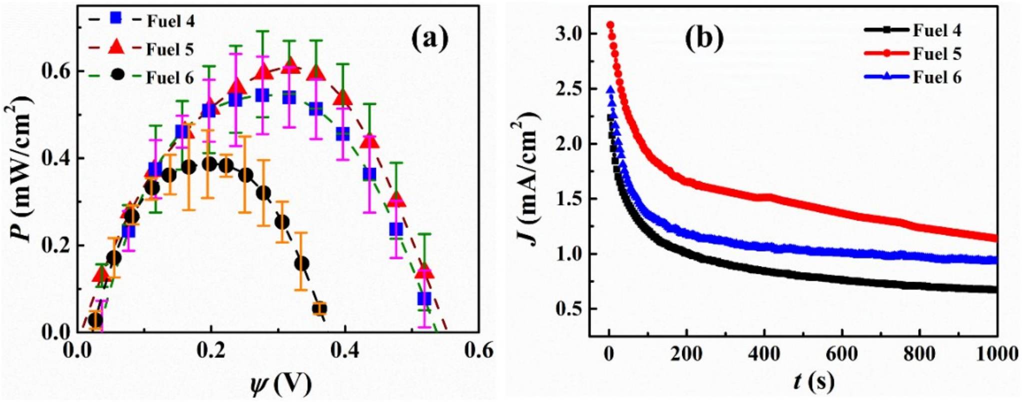

Figure S6. The plot (a) shows *P*-*ψ* characteristics of μ-DropFC with Fuels 4 – 6 containing the organic pollutant, Rhodamine (Rh6G). The plot (b) shows the chronoamperometric current density (*J*) versus time (*t*) studies for the same μ-DropFCs at an applied potential of 0.1 V. The plots correspond to the Fuels 4 – 6 in the Table 1 of the main manuscript.

The μ-DropFC was also capable of functioning as a dye degradation setup without compromising significantly on its energy production capabilities. In order to prove this aspect, we added a fixed amount of an aqueous solution of Rhodamine 6G (Rh6G) (0.5 mg/mL) in the μ-

DropFC to prepare the Fuels 4 – 6, described in the Table 1 of the main manuscript. The plot (a) in the **Figure S6** show that in presence of additives such as Au NPs (Fuel 5) and Au/CdS NPs (Fuel 6), the μ-DropFC was able to generate decent $P_{max} \sim 0.61$ and 0.51, respectively. Even without these additives also the Fuel 4 produced a slightly lower P_{max} while simultaneously performing the dye degradation. The plot (b) shows the chronoamperometric current density (J) – time (t) studies for μ-DropFC at an applied potential of 0.1 V in presence of Rh6G solution (0.5 mg/mL). Again, as expected, the system containing only dye molecules displayed the least amount of current density.

However, on addition of Au and/or CdS NPs there was significant improvement in which use of Au NPs showed maximum energy harvesting. In a way, the Au/CdS NP system showed effective photocatalytic properties for the dye degradation.[5,6] Under the illuminated conditions, these photocatalysts degraded the organic dye molecules by breaking down their backbone. Subsequently, rather than facilitating the breakdown of the peroxide fuel at the electrodes, the additives engaged in dye degradation. Thus, when only Au NPs were present, the setup showed a higher J value wherein the rate of energy harvesting was larger and rate of dye degradation was rather less. However, for Au/CdS NPs, the dye degradation rate was faster while the rate of energy harvesting was found to be little less. Importantly, these effects stabilized the cell in relation to the J values because a stable current density could be achieved for a long period of time, as shown in plot (b).

V. Effect of Additive Volumes on *P*-*ψ*

The plot (a) **Figure S7** shows the case studies wherein different volumes of Au/CdS NP solutions 10 μL to 80 μL was added to Fuel 1 and the variation in the P_{max} was noted down. The plot suggests that increasing the volume of the NP increased P_{max}, however, the increase was not always linear. As the volume increased, the reactants delivered to the electrodes increased, which increased the rate of reaction and hence P_{max}. However, this also increased the diffusional resistance faced by the different species and once this effect was prominent the P_{max} values saturated. Plot (b) shows that the increase in P_{max} was rather more significant when only the Au NPs volume proportion was increased in the peroxide fuel. However, in this plot too, we observed that the peak power density tends to saturate at higher solution volume. From these results, the adequate volume of NPs required for a single cell in order to obtain a high power density was optimized. Hence, we utilized around 70 μL of solution for every cell in the VLSI system to get the maximum power density in an optimal manner.

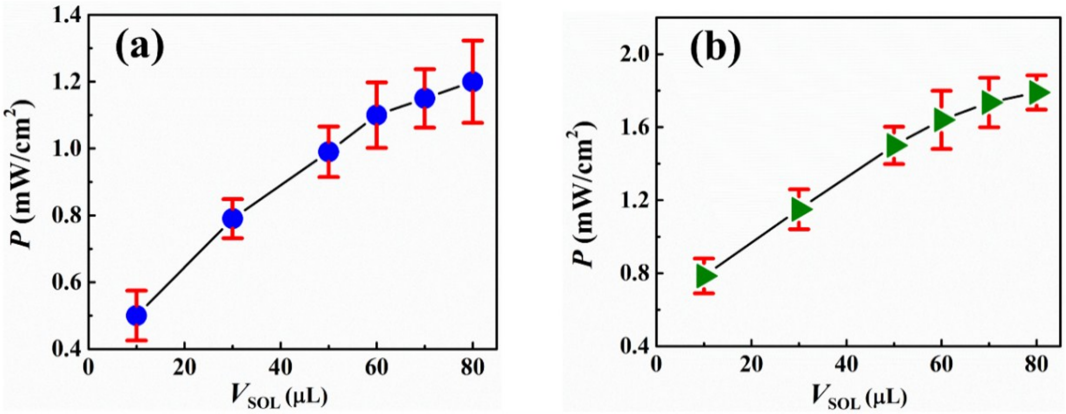

Figure S7: Plots show the variation of P_{max} with varying volume of fuels (V_F). Image (a) depicts the effects of the volume of Au/CdS NP solutions while image (b) reveals the effects of the volume of Au NP solutions.

VI. Efficiency Calculations

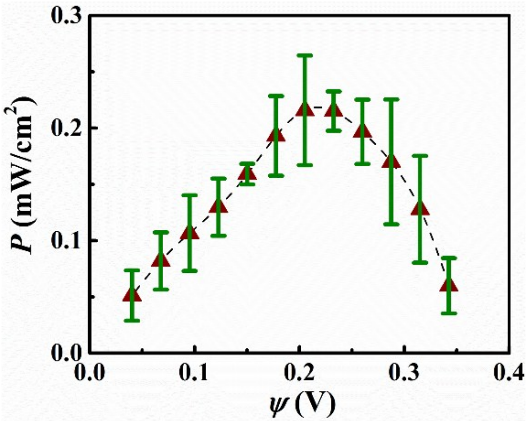

Figure S8: Plot showing the variation of P with ψ for the μ-DropFC under dark condition for when Fuel 1 was employed.

Effect of the incoming radiations was analyzed by performing the power-potential analysis for the μ-DropFC system employing Fuel 1, under dark condition. As can be observed by the **Figure S8,** very less P values from the system could be obtained as compared to the condition when the system was operating under external radiations. Thus, the incoming external waves not only had influence on the overall current generation but also on the overall potential value. Furthermore, in order to evaluate the performance criteria for the μ-DropFC system, the overall efficiency of the the μ-DropFC was determine employing the following formula:

$$\varepsilon_O = \varepsilon_T \times \varepsilon_E \times \varepsilon_{PV} \ . \tag{9}$$

where, ε_O is the overall efficiency of the system, ε_T is the thermodynamic efficiency of the system, ε_E is the electrochemical efficiency and ε_{PV} is the photovoltaic efficiency of the system. The thermodynamic efficiency of the system represents the overall allowed driving force for the redox reactions owing due to the inherent chemical energy of the fuel utilized. The electrochemical efficiency of the system represents the maximum driving force involved during the fuel cell operation as it takes into consideration the different over potentials involved and the corresponding losses occurring due to them. The photovoltaic efficiency highlights the increment in the overall charge transfer processes due to the presence of external radiation. Briefly, these efficiencies can be represented by:

$$\varepsilon_T = \frac{\Delta G}{\Delta H} \ , \tag{10}$$

$$\varepsilon_E = \frac{\psi_{oc}}{\psi_{th}} \ , \tag{11}$$

$$\varepsilon_{PV} = \frac{\psi_{max} \times J_{max}}{P_{in}} \ . \tag{12}$$

Here, ΔG and ΔH represent the free energy and enthalpy values of the overall hydrogen peroxide disproportion reaction.[7,8] It has been assumed that the enthalpy of the reaction and free energy values for the system does not vary significantly upon addition of the different additives. The parameters ψ_{oc} and ψ_{th} represents the open-circuit potential and the actual redox potential of the system under standard conditions. The parameters J_{max} and ψ_{max} represents the maximum current density achieved by the system at the corresponding applied potential and P_{in} represents the input energy of the system due to external radiations. For the proposed systems, the values for the different parameters corresponding to the different fuels have been laid out in the Table 4 of the main manuscript. For a particular fuel composition, in this case Fuel 2I, the parametric values which determine the overall μ-DropFC efficiency have been given as follows: ΔG = 120 kJ/mol, ΔH = 190 kJ/mol, ψ_{oc} = 0.58 V, ψ_{th} = 1.08 V, $\psi_{max} \times J_{max}$ = 0.8 W/cm^2 and P_{in} = ~70 mW/cm^2. The efficiencies of the system were determined utilizing equations (9) – (12). In all the calculations, the area has been taken to be the circular footprint of the droplet of diameter 5 ± 1 mm.

VII. Description of Videos

Supplementary Video 1: Arrangement of the overall μ-DropFC setup has been demonstrated in this video. Fuel cell characterization has been carried out using a linear sweep voltammetry technique with the help of a Keithley sourcemeter. A Xe lamp (light source) has been employed for illuminating the system from the top as shwon.

Supplementary Video 2: Performance of the μ-DropFC in terms of its open-circuit voltage has been displayed in the dark and illuminated conditions. For clearly highlighting the effect of the external radiation, a higher concentration of constituents has been employed than the usual. The video shows that the incoming light did increase the overall output value of the μ-DropFC system, as is shown by the multimeter reading.

References

(1) An, L.; Zhao, T.; Yan, X.; Zhou, X.; Tan, P. The Dual Role of Hydrogen Peroxide in Fuel Cells. *Sci. Bull.* **2015**, *60*, 55–64.

(2) Yamazaki, S.; Siroma, Z.; Senoh, H.; Ioroi, T.; Fujiwara, N.; Yasuda, K. A Fuel Cell with Selective Electrocatalysts Using Hydrogen Peroxide as Both an Electron Acceptor and a Fuel. *J. Power Sources* **2008**, *178*, 20–25.

(3) Fukuzumi, S.; Yamada, Y. Hydrogen Peroxide Used as a Solar Fuel in One-Compartment Fuel Cells. *ChemElectroChem* **2016**, *3*, 1978–1989.

(4) Suwathy, R.; Reddy, K. M.; Pramoth Kumar, M.; Venkatesan, M. Droplet Impinging Behavior on Surfaces Part I - Hydrogen Peroxide on Aluminium Surface. *IOP Conf. Ser. Mater. Sci. Eng.* **2016**, *149*, 012219.

(5) Jiao, Y.; Ma, X.-M.; Wang, F.-F.; Wang, K.; Zhang, P.-P.; Wang, Z.-Z.; Yang, L. Facile and Low-Cost Synthesis of Gold Nanoparticles Supported on Cadmium Sulphide Flower-like Three-Dimensional Assemblies. *Micro Nano Lett.* **2012**, *7*, 631-635.

(6) Torimoto, T.; Horibe, H.; Kameyama, T.; Okazaki, K.; Ikeda, S.; Matsumura, M.; Ishikawa, A.; Ishihara, H. Plasmon-Enhanced Photocatalytic Activity of Cadmium Sulfide Nanoparticle Immobilized on Silica-Coated Gold Particles. *J. Phys. Chem. Lett.* **2011**, *2*, 2057–2062.

(7) Disselkamp, R. S. Can Aqueous Hydrogen Peroxide Be Used as a Stand-Alone Energy

Source? *Int. J. Hydrogen Energy* **2010**, *35*, 1049–1053.

(8) Sanli, A. E.; Aytaç, A. Response to Disselkamp: Direct Peroxide/Peroxide Fuel Cell as a Novel Type Fuel Cell. *Int. J. Hydrogen Energy* **2011**, *36*, 869–875.